Iranian Journal of Astronomy and Astrophysics
Vol. 13, No. 1, Winter 2026, 1–14
©Available online at http://ijaa.du.ac.ir
DOI: 10.22128/ijaa.2026.3417.1254
Online ISSN: 2383–403X

Iranian Journal of Astronomy and Astrophysics

Research Paper

Data-Driven Forecasting of Solar and Geomagnetic Activity Using Relative Sunspot Numbers

Sevim Ranjbar[1] · Somayeh Taran*[2]
[1] Faculty of Physics, University of Tabriz, PO Box 51666-16471, Tabriz, Iran;
email: sevimranjbar1403@ms.tabrizu.ac.ir
[2] Faculty of Physics, University of Tabriz, PO Box 51666-16471, Tabriz, Iran;
*email: taran@tabrizu.ac.ir

Received: 7 August 2026; **Accepted:** 13 September 2026; **Published:** 19 September 2026

Abstract. Accurate modeling and forecasting of solar and geomagnetic activity is essential for advancing our fundamental understanding of solar-terrestrial interactions and magnetospheric dynamics. In this study, we propose a computational approach based on a Long Short-Term Memory (LSTM) neural network for predicting the 10.7 cm solar radio flux (F10.7) and four widely used geomagnetic indices (K_p, Dst, ap, and AE) using the Relative Sunspot Number (RSSN) as the primary input. To enhance the model's predictive capability, we introduce a physically motivated feature engineering strategy that incorporates nonlinear and temporal characteristics of solar dynamics, including quadratic and rolling-average features, as well as autoregressive information for each target variable. We employ a strictly leak-free Purged-Embargo validation strategy to prevent information leakage during model development. We evaluate the framework using hourly observations from 1 January 2000 to 10 January 2026, covering Solar Cycles 23, 24, and 25. Our proposed model achieves excellent predictive performance for the F10.7 and Dst indices, with coefficients of determination R^2 of 0.9639 and 0.9584, respectively. Good agreement is also obtained for the K_p and ap indices ($R^2 = 0.8642$ and 0.8622), while the more dynamic AE index reaches an R^2 of 0.6939. These results demonstrate that the proposed framework provides an accurate and robust approach for forecasting solar and geomagnetic activity from a minimal set of input observations.

Keywords: Solar-Terrestrial Interactions, Geomagnetic Indices, Time-Series Modeling, Relative Sunspot Number.

1 Introduction

Solar activity is governed by the evolution of the solar magnetic field and manifests through a wide range of phenomena, including sunspots, solar flares, coronal mass ejections (CMEs), and high-speed solar wind streams [1–3]. Among these manifestations, the sunspot number (SSN) remains the longest and most reliable observational proxy of solar magnetic activity, providing a continuous record spanning more than four centuries [4–6]. The approximately 11-year Schwabe solar cycle, characterized by the periodic rise and fall of sunspot numbers, modulates the interplanetary magnetic field (IMF), solar wind properties, and the flux of

* *Corresponding author*

energetic particles reaching Earth's magnetosphere [7,8]. These variations drive geomagnetic disturbances that are routinely monitored through planetary geomagnetic indices such as *ap*, *aa*, K_p, *Dst*, and SYM-H, each quantifying different aspects of the magnetosphere's response to solar forcing [9,10]. Consequently, geomagnetic indices provide an integrated record of solar-terrestrial interactions and constitute valuable indirect proxies of solar activity. Despite their common solar origin, the relationship between sunspot activity and geomagnetic disturbances is neither linear nor stationary [11,12].During the declining phase of the solar cycle, geomagnetic activity is increasingly influenced by recurrent high-speed solar wind streams from coronal holes, rather than CMEs. This causes geomagnetic indices to show delayed, shifted, or double-peaked responses compared to the sunspot cycle, reflecting both solar activity intensity and changing energy transfer mechanisms from the solar wind to Earth's magnetosphere. Understanding these relationships is crucial for heliophysics and space weather forecasting [13–15].

The geomagnetic precursor method introduced by [16] demonstrated that geomagnetic activity near solar minimum provides a reliable predictor of the amplitude of the subsequent solar cycle. This approach was subsequently refined by [17], who proposed using the minimum value of the aa index, and further developed through the decomposition of geomagnetic activity into transient and recurrent components by [18]. Modern reassessments have confirmed that geomagnetic precursor techniques remain among the most successful empirical methods for predicting solar cycle amplitude [19,20].

Long-term statistical analyses further revealed that the coupling between solar and geomagnetic activity evolves over time. Using more than a century of observations, [21] showed that although annual sunspot numbers and the *aa* index follow the same 11-year cycle, their correlation has gradually weakened while the temporal lag between them has increased. Similar conclusions were reached by [12], who compared multiple solar and geomagnetic indices and demonstrated that IMF variations correlate more strongly with geomagnetic activity than sunspot numbers alone, emphasizing the multivariate nature of solar-terrestrial coupling.

Beyond conventional correlation analysis, numerous studies have employed regression, spectral, and nonlinear time-series techniques to characterize solar–geomagnetic relationships. Multiple regression analyses demonstrated that combining geomagnetic and solar indices substantially improves the prediction of temporal variation of the ground magnetic field [22]. Continuous wavelet analysis revealed common periodicities near the Schwabe cycle together with additional spectral components unique to geomagnetic activity, reflecting the influence of recurrent solar wind structures and IMF variability [23]. Cross-wavelet and lag-correlation studies further showed that the phase relationship between solar and geomagnetic activity depends strongly on temporal scale and solar-cycle phase [12,24]. Moreover, investigations of geomagnetic storms have consistently shown that the most intense disturbances often occur during the declining phase of the solar cycle despite decreasing sunspot numbers, highlighting the important role of CMEs, coronal holes, and high-speed solar wind streams beyond sunspot activity alone [25].

Collectively, these studies demonstrate that geomagnetic indices contain substantial information regarding the temporal evolution of solar magnetic activity. However, most classical statistical approaches rely on assumptions of linearity, stationarity, or fixed temporal relationships that cannot fully represent the highly nonlinear dynamics of the coupled solar-terrestrial system. The growing availability of continuous solar wind observations, long-term geomagnetic records, and advances in computational power have therefore stimulated the adoption of machine learning (ML) methods capable of learning complex nonlinear relationships directly from observations.

The limitations of conventional statistical approaches have stimulated growing interest in machine learning (ML) techniques, which are well suited to modeling the nonlinear and nonstationary relationships characteristic of solar-terrestrial interactions. Benefiting from the increasing availability of long-term observational datasets and advances in computational power, ML methods have become an important component of modern heliophysics and space weather forecasting [26–29]. Deep learning architectures, including recurrent neural networks (RNNs), long short-term memory (LSTM) networks, gated recurrent units (GRUs), convolutional neural networks (CNNs), and hybrid frameworks, have demonstrated remarkable success in predicting geomagnetic indices from solar wind and IMF observations, consistently outperforming many traditional empirical and statistical models in forecasting accuracy [27,30].

The increasing availability of benchmark datasets has further accelerated the development of machine-learning models for data-driven space weather forecasting. The NOAA MagNet competition [31] established a standardized framework for short-term Dst prediction, where the best-performing ensemble deep-learning models achieved root-mean-square errors of approximately 11 nT. Similarly, [32] demonstrated that LSTM networks can accurately predict the onset of geomagnetic storms one hour in advance by exploiting solar-wind plasma, interplanetary magnetic field, and magnetic-helicity measurements, while [33] further improved short-term Dst forecasting using a hybrid LSTM–Storm architecture, achieving correlation coefficients exceeding 0.95 and root-mean-square errors below 9 nT for prediction horizons of up to six hours. In parallel with efforts focused on the Dst index, data-driven methodologies have also been successfully implemented for forecasting other essential planetary metrics; notably, [34] recently developed a robust time-series framework specifically dedicated to predicting the K_p index. Beyond deep learning, ensemble methods such as Random Forest, Gradient Boosting, Extreme Gradient Boosting (XGBoost), and LightGBM have also demonstrated competitive forecasting skill while offering valuable insights into feature importance and model interpretability [27,31].

The remainder of this paper is organized as follows. Section 2 describes the data, Section 3 presents the methodology, Section 4 reports the results, Section 5 discusses the findings, and Section 6 concludes the paper.

2 Data

In this study, we use the relative sunspot number (RSSN) as the input parameter for predicting geomagnetic activity indices including the planetary geomagnetic index k_p, the disturbance storm time index (Dst), the planetary amplitude index (ap), the auroral electrojet index (AE), and the solar radio flux at 10.7 cm (F10.7) . The (RSSN) is one of the longest and most widely used measures of solar activity and is defined by

$$RSSN = K(10g + s), \tag{1}$$

where g, s, K are the number of sunspot groups, the total number of individual sunspots, and an observer-dependent correction factor introduced to normalize observations to the original Wolf sunspot scale, respectively [6,35]. This formulation provides a consistent long-term record of solar magnetic activity and has been extensively employed in studies of solar variability and solar–terrestrial interactions.

The geomagnetic indices represent different aspects of solar and geomagnetic activity, the (K_p) index is a global 3-hour planetary index derived from measurements at 13 mid-latitude geomagnetic observatories, while the ap index is its linear equivalent expressed in units of 2 nT. The Dst index is computed from low-latitude geomagnetic observatories and measures the intensity of the magnetospheric ring current during geomagnetic storms. The

AE index quantifies auroral electrojet activity using observations from high-latitude magnetometer stations and serves as an indicator of magnetosphere–ionosphere coupling [36]. These parameters are provided as hourly averages and span 1 January 2000 to 10 January 2026 covering the descending phase of Solar Cycle 23, the entire Solar Cycle 24, and the rising, maximum, and early declining phases of Solar Cycle 25. This interval encompasses periods of both low and high solar activity, providing a comprehensive dataset for investigating the relationship between solar activity and geomagnetic indices. We obtain all data from the OMNIWeb interface (`https://omniweb.gsfc.nasa.gov/`).

3 Methods

3.1 Data Preprocessing and Feature Engineering

To improve the forecasting capability of the proposed framework while ensuring a strictly leak-free learning process, we construct a set of physically motivated input features that capture both the nonlinear response of solar activity and the temporal memory of the solar-terrestrial system. The hourly RSSN is adopted as the primary predictor, from which several complementary features are derived.

We introduce a squared sunspot feature (RSSN^2) to represent the well-established nonlinear relationship between sunspot activity and continuous solar indices, most notably F10.7. Physically, even during deep solar minimum (RSSN = 0), thermal emission from the quiet solar atmosphere maintains a background radio flux of approximately 65–67 solar flux units (sfu). In contrast, during periods of intense activity, the increase in F10.7 becomes progressively weaker due to saturation effects. Consequently, this relationship is commonly approximated by a second-order polynomial [37,38]. Motivated by this well-established nonlinear behavior, we approximate the relationship between the RSSN and the prediction target $\mathrm{y}_{\mathrm{target}}$ using a second-order polynomial,

$$\mathrm{y}_{\mathrm{target}} \approx \mathrm{A} + \mathrm{B} \times \mathrm{RSSN} + \mathrm{C} \times \mathrm{RSSN}^2, \tag{2}$$

where A, B, and C are empirical coefficients. Rather than imposing this functional form through fixed coefficients, we include the RSSN^2 term as an additional input feature, allowing the neural network to learn the underlying nonlinear relationship directly from the data. This strategy provides greater flexibility by enabling the model to adapt the quadratic dependence according to the characteristics of each prediction target. Although the quadratic relationship between the sunspot number and the F10.7 radio flux is the best-established example in the literature [37,38], we retain the RSSN^2 feature for all solar and geomagnetic prediction tasks. Using a common feature set across all targets ensures methodological consistency and facilitates a fair comparison of model performance within a unified learning framework.

A key advantage of this approach is that the LSTM automatically learns the contribution of each input feature during training through gradient-based optimization. This includes the nonlinear RSSN^2 term, whose importance is determined separately for each prediction target. As a result, the model can exploit nonlinear information whenever it improves predictive performance, without requiring manually designed, target-specific feature engineering. If the quadratic term contains little useful information for a particular index, the network naturally reduces its influence by assigning it smaller weights during training. On the other hand, when the nonlinear feature provides meaningful predictive information, its contribution is strengthened automatically. This adaptive learning process enables a single, unified feature space to be applied across all prediction tasks while allowing the model to tailor the effective use of each feature according to the underlying physical relationships present in the data. This flexibility is also physically well motivated. Geomagnetic activity does not respond linearly to solar activity but arises from a complex chain of coupled processes involving the Sun, the solar wind, and the Earth's magnetosphere [39,40]. By retaining the RSSN^2 feature, the model is given additional capacity to learn these nonlinear relationships directly from the data, wherever they exist. At the same time, because the neural network determines the importance of each feature during training, it is not constrained by a fixed empirical formula. Instead, it can adaptively capture nonlinear behavior only when it improves the prediction, resulting in a more flexible and physically meaningful representation of the solar-terrestrial system.

To capture the long-term influence of persistent solar active regions, we also derive a temporal feature from the RSSN time series. Active regions, sunspot groups, and plages can remain visible over one or more solar rotations, continuing to modulate the level of solar activity. Since the synodic (Carrington) rotation period of the Sun is approximately 27 days [41], this timescale provides a physically meaningful window for representing the accumulated history of solar activity.

Accordingly, we compute a causal rolling mean over 648 hours (27×24 h),

$$\mu_t = \frac{1}{W} \sum_{i=0}^{W-1} x_{t-i}, \tag{3}$$

where $W = 648$ and x_t denotes the RSSN at time t. The rolling average is calculated using only the current and past observations, ensuring that no future information is incorporated into the feature. Consequently, the resulting temporal feature is strictly causal and completely avoids information leakage, while providing the model with a physically motivated measure of the background level of solar activity over the previous solar rotation.

To better represent the temporal persistence of geomagnetic activity, we also include autoregressive features for each prediction target. Geomagnetic indices are well known to exhibit memory effects, especially during the main and recovery phases of magnetic storms, where current conditions are strongly influenced by their recent history. To account for this behavior, the input feature set includes both the previous value of the target variable ($\mathrm{y_t}$) and its 24-hour causal rolling mean. Together, these features provide the network with information on both the immediate state of the system and its longer-term evolution, enabling it to capture rapid variations as well as the gradual recovery following geomagnetic disturbances.

Finally, all input features and target variables are standardized using Z-score normalization,

$$z = \frac{x - \mu_{\text{train}}}{\sigma_{\text{train}}}, \tag{4}$$

where μ_{train} and σ_{train} are the mean and standard deviation computed exclusively from the training subset. Estimating these normalization parameters only from the training data prevents information leakage into the validation and test sets. In addition, standardization places all variables on a common numerical scale, improving training stability, facilitating gradient-based optimization, and promoting faster convergence of the neural network.

3.2 Sliding Window Generation and Purged-Embargo Splitting

We convert the multivariate time series into a collection of overlapping input–target pairs using a sliding-window approach, with window lengths w ranging from 1 to 100 hours. For each sample, the model receives the observations from the previous w hours (up to time t)

and predicts the target variable one hour later, at time $t + 1$. This formulation allows the network to learn temporal dependencies over a range of historical contexts while addressing a one-hour-ahead forecasting problem. Figure 1 illustrates the overall windowing and data-splitting procedure.

A random split of these overlapping windows would lead to severe data leakage because neighboring samples share much of the same information. As a result, nearly identical sequences could appear in both the training and evaluation sets, producing overly optimistic performance estimates. To avoid this issue and preserve the chronological nature of the forecasting task, we employ a strictly leak-free Purged-Embargo splitting strategy. The original time series is first partitioned sequentially into training (70%), validation (15%), and testing (15%) subsets. This chronological partitioning ensures that the model is trained only on past observations, while all future data remain completely unseen during model training, hyperparameter tuning, and final performance evaluation.

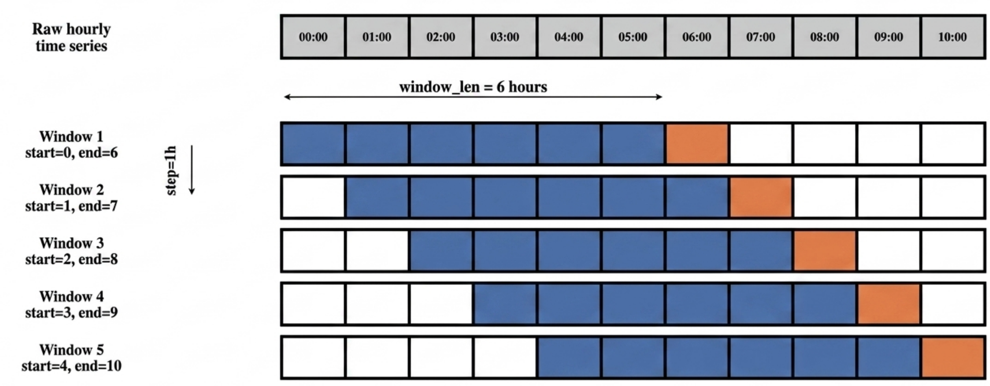

Figure 1: Schematic illustration of the sliding-window approach used to construct the input–target pairs for LSTM training. The raw hourly time series is segmented into overlapping input windows of length $w = 6$ hours (blue), which are shifted forward by one hour (step = 1). For each window, the model uses the previous six hourly observations to predict the value at the following hour (orange).

3.3 LSTM Model Architecture and Training Framework

The proposed computational framework is based on a two-layer LSTM network, which is well suited for modeling the temporal evolution of solar and geomagnetic time-series data. We summarize the complete data-processing and model-training workflow in Figure 2.

As shown in Figure 2, the analysis begins by setting fixed random seeds to ensure reproducibility before loading the RSSN data and the corresponding target indices. Feature engineering is then performed by generating the raw, smoothed, and squared RSSN features, followed by the inclusion of target-history variables. All predictors are subsequently normalized using the statistics of the training set only, thereby preventing information leakage.

The normalized data are converted into supervised learning samples by constructing sliding windows for a given input window size. These samples are then divided into training, validation, and testing subsets using a chronological time-based split. If the selected window size provides sufficient training samples, the LSTM model is trained and its predictive performance is assessed using the coefficient of determination (R^2) and the root-mean-square error (RMSE). The predictions are stored, and the same procedure is repeated for all predefined window sizes. Finally, the performance metrics are collected to identify the optimal temporal configuration for each prediction task.

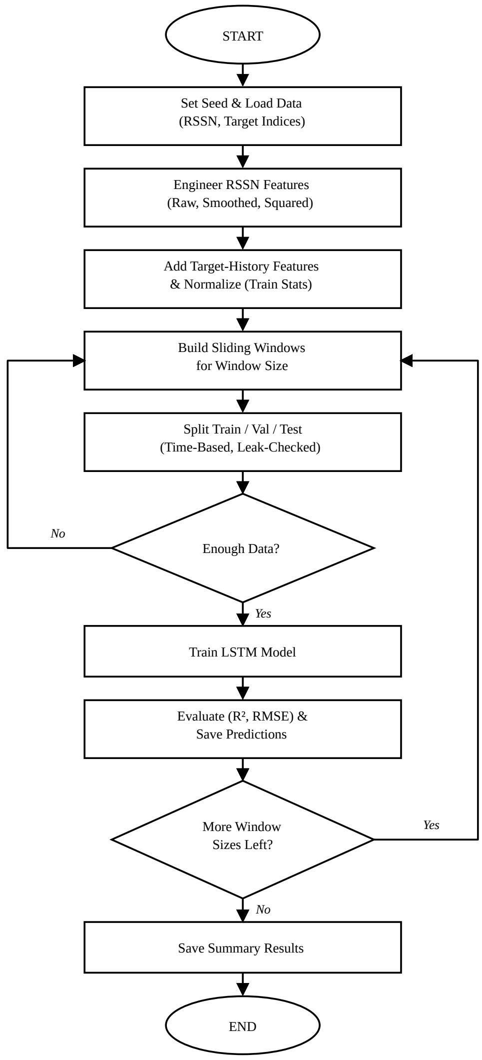

Figure 2: End-to-end workflow of the proposed forecasting framework. The pipeline includes data initialization, feature engineering, normalization, sliding-window construction, chronological train–validation–test splitting, LSTM training and evaluation, and an iterative search over different input window sizes.

The network parameters are optimized using the Adam optimizer with an initial learning rate of 5×10^{-4}. Because solar and geomagnetic activity occasionally exhibits large excursions during disturbed conditions, the Huber loss function is adopted to improve robustness against outliers while maintaining accurate fitting for the majority of samples. It is defined as

$$L_\delta(y, \hat{y}) = \begin{cases} \frac{1}{2}(y - \hat{y})^2 & \text{for } |y - \hat{y}| \le \delta \\ \delta|y - \hat{y}| - \frac{1}{2}\delta^2 & \text{otherwise} \end{cases} \quad (5)$$

where y and $\hat{y}$ denote the true and predicted values, respectively, and $\delta = 1.0$. The model is trained for a maximum of 60 epochs with early stopping and adaptive learning-rate reduction, allowing efficient convergence while reducing the risk of overfitting. The model is trained for a maximum of 60 epochs using the Adam optimizer, with early stopping and adaptive learning-rate reduction to improve convergence and reduce overfitting.

The predictive performance of the model is assessed using the root mean square error (RMSE) and the coefficient of determination (R^2), defined as

$$\mathrm{RMSE} = \sqrt{\frac{1}{n}\sum_{i=1}^{n}(y_i - \hat{y}_i)^2}, \quad (6)$$

$$R^2 = 1 - \frac{\sum_{i=1}^{n}(y_i - \hat{y}_i)^2}{\sum_{i=1}^{n}(y_i - \bar{y})^2}, \quad (7)$$

where y_i and $\hat{y}_i$ are the observed and predicted values, respectively, and $\bar{y}$ is the mean of the observed values.

4 Results

In this section, we evaluate the performance of the proposed LSTM framework for predicting the F10.7 solar radio flux and the geomagnetic indices (K_p, ap, Dst, and AE) from the RSSN. The analysis is based on hourly observations spanning the period from 1 January 2000 to 10 January 2026, encompassing a wide range of solar activity conditions across Solar Cycles 23, 24, and 25. We first investigate the influence of the input window length on the forecasting performance and determine the optimal temporal context for each target variable. The optimized models are then evaluated on the independent test set using the performance metrics introduced in the previous section, followed by a comparison between the observed and predicted time series.

4.1 Optimal Window Size Selection

To investigate the influence of the historical context on forecasting performance, we trained the proposed model using input window lengths ranging from 1 to 100 hours. Figure 3 presents the corresponding R^2 scores (left panel) and RMSE values (right panel) for each prediction target as a function of the input window length.

Overall, both performance metrics remain remarkably stable across the entire range of window lengths, indicating that the proposed LSTM framework is largely insensitive to the exact choice of historical context. The Dst index consistently achieves the highest predictive accuracy, with R^2 values close to 0.95 and the lowest RMSE of approximately 4.8. The F10.7 index also exhibits excellent performance, maintaining R^2 values above 0.90 with RMSE values typically between 8 and 12, although a few isolated window lengths produce slightly larger prediction errors. The K_p and ap indices display similarly stable behavior, with nearly constant R^2 values around 0.85 and correspondingly low and nearly unchanged RMSE values across all window lengths. In comparison, the *AE* index consistently yields the lowest R^2 values (∼0.68–0.69) and the largest RMSE (∼118), reflecting the greater difficulty of predicting its highly variable behavior.

The close agreement between the R^2 and RMSE trends demonstrates that changes in the input window length have only a minor impact on forecasting performance. Consequently, the optimal window length for each target was selected based on the combination of the highest R^2 and the lowest RMSE and was adopted for all subsequent analyses.

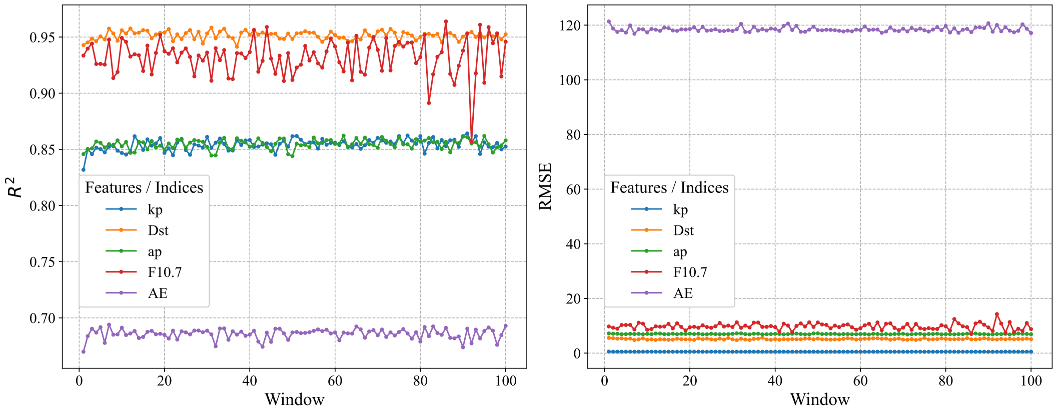

Figure 3: Variation of the coefficient of determination (R^2, left panel) and the root mean square error (RMSE, right panel) as a function of the input window length for predicting the K_p, Dst, ap, F10.7, and AE indices.

Table 1 summarizes the optimal input window selected for each prediction target together with the corresponding highest R^2 score and lowest RMSE obtained on the independent test set. The optimal window lengths vary among the indices, ranging from 7 hours for AE to 91 hours for K_p, indicating that the amount of historical information yielding the best predictive performance differs slightly for each target.

Among all variables, the proposed model achieves its highest predictive accuracy for the F10.7 solar radio flux and the Dst index, with maximum R^2 values of 0.9639 and 0.9584 obtained using window lengths of 86 and 31 hours, respectively. The K_p and ap indices are also predicted with good accuracy, reaching R^2 values of 0.8642 and 0.8622 at optimal window lengths of 91 and 62 hours. In comparison, the AE index is the most challenging target, yielding the lowest predictive performance with a maximum R^2 of 0.6939 and an optimal window length of 7 hours. Despite these differences, all indices achieve their best performance within the investigated range of window sizes, demonstrating that the proposed framework can effectively adapt to different temporal characteristics of solar and geomagnetic activity.

4.2 Time Series Forecasting Analysis

Figure 4 compares the observed and predicted time series for the five target variables over the independent test period. Overall, the proposed LSTM framework successfully reproduces the temporal evolution of all indices, demonstrating its ability to capture both the long-term variability and the short-term fluctuations of solar and geomagnetic activity.

Table 1: Optimal Window Sizes and Best Performance Metrics for Space Weather Indices

Index	Optimal Window	Highest R^2	Lowest RMSE
F10.7	86	0.9639	7.1725
Dst	31	0.9584	4.7568
K_p	91	0.8642	0.4929
ap	62	0.8622	6.8131
AE	7	0.6939	116.8453

The F10.7 solar radio flux exhibits the closest agreement between the observations and predictions. The model accurately reproduces the gradual variations associated with the solar cycle, as well as the majority of short-term enhancements, consistent with the high R^2 value reported in Table 1. Similarly, the Dst index is predicted with high accuracy. The model successfully follows both quiet geomagnetic conditions and the occurrence of major storm events, although the largest negative excursions are occasionally underestimated.

The predictions for the K_p and ap indices also show good agreement with the observations. For both indices, the model captures the overall variability and the timing of enhanced geomagnetic activity, while exhibiting only minor discrepancies during periods of intense disturbances. In particular, the strongest peaks are slightly smoothed, a common characteristic of regression-based forecasting models.

Among the five targets, the AE index presents the greatest forecasting challenge. Although the model reproduces the overall temporal behavior and follows the occurrence of enhanced auroral activity, it tends to underestimate the magnitude of the most extreme and rapidly varying electrojet intensifications. This behavior is expected given the highly intermittent and nonlinear nature of the AE index, which is strongly influenced by short-lived substorm processes that are difficult to infer from the RSSN alone.

Overall, the close correspondence between the observed and predicted time series confirms that the proposed framework effectively captures the dominant temporal characteristics of solar and geomagnetic variability, while maintaining robust predictive performance across a wide range of activity levels.

5 Discussion

The results demonstrate that the proposed LSTM framework can effectively learn the relationship between the RSSN and several key solar and geomagnetic indices. Among the five targets, the highest predictive accuracy is achieved for the F10.7 radio flux and the Dst index, followed by the K_p and Ap indices, whereas the AE index remains the most challenging to predict. This trend is consistent with the underlying physical processes governing these parameters.

The excellent performance obtained for the F10.7 index is not surprising, as both RSSN and F10.7 originate from solar magnetic activity and are known to exhibit a strong nonlinear relationship over multiple solar cycles [37,38]. Unlike traditional empirical approaches that explicitly assume a quadratic relationship, our model learns this dependence directly from the data, enabling it to capture both long-term solar-cycle variability and shorter-term fluctuations.

The high accuracy achieved for the Dst index is also consistent with previous studies showing that LSTM networks are well suited for forecasting geomagnetic storms because they can effectively model the temporal evolution of the magnetospheric ring current [27,42].

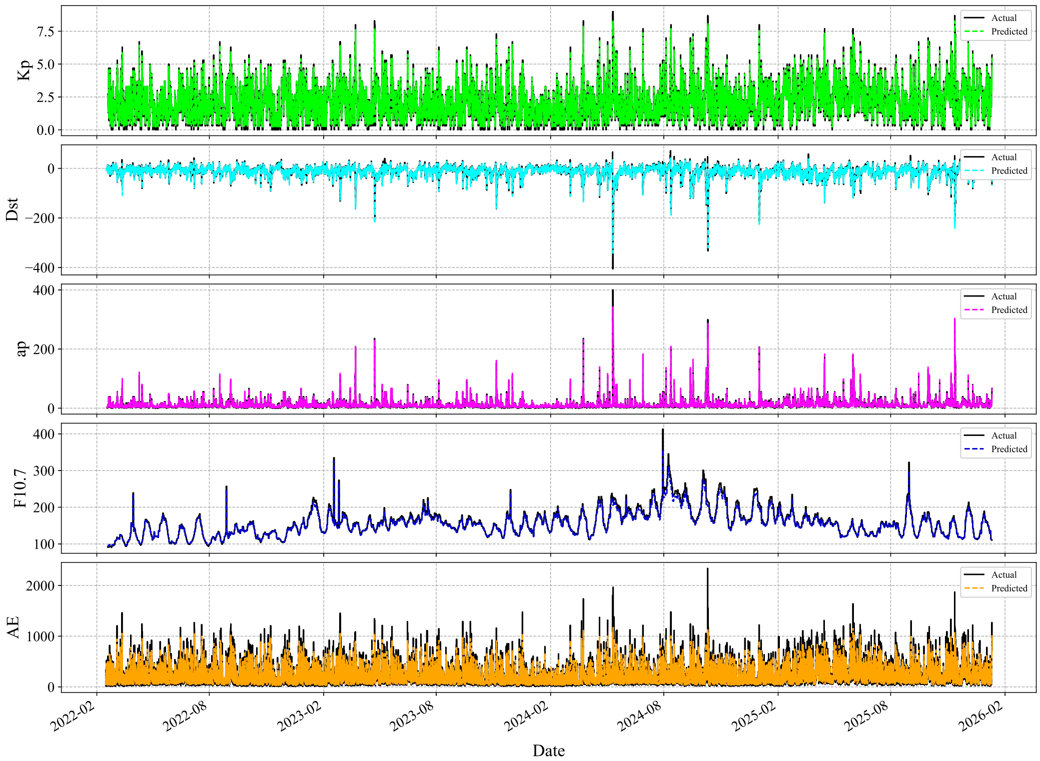

Figure 4: Comparison between the observed (black solid lines) and predicted (colored dashed lines) time series for the five target variables (K_p, Dst, ap, F10.7, and AE) on the independent test set from February 2022 to January 2026.

While many existing machine-learning models rely on solar-wind parameters such as the interplanetary magnetic field and solar-wind velocity as input features [31,42], the present study demonstrates that competitive forecasting performance can be achieved using only the RSSN together with physically motivated feature engineering. In comparison, the lower performance obtained for the K_p, ap, and particularly the AE index is expected. These indices are influenced not only by the overall level of solar activity but also by rapidly changing solar-wind conditions and magnetosphere–ionosphere coupling processes that cannot be fully inferred from the sunspot number alone [40,43]. Consequently, although the model successfully reproduces the overall temporal evolution of these indices, it tends to smooth the most extreme events, especially for the highly variable AE index.

Finally, the relatively small changes in forecasting performance over the range of input window lengths indicate that the proposed framework is robust to the choice of historical context. This robustness, together with the strict Purged-Embargo validation strategy adopted in this work, suggests that the reported performance provides a reliable estimate of the model's generalization ability. Future work will investigate the incorporation of additional solar observations and high-resolution solar-wind measurements to further improve the prediction of rapidly varying geomagnetic activity and significant solar-terrestrial phenomena.

6 Conclusion

In this work, we developed an LSTM-based framework for predicting the F10.7 solar radio flux and four widely used geomagnetic indices (K_p, Dst, ap, and AE) using the Relative Sunspot Number (RSSN) as the primary input. By combining physically motivated feature engineering with a leak-free Purged-Embargo validation strategy, the proposed approach provides a reliable framework for modeling the nonlinear relationship between solar activity and geomagnetic variability.

The model achieved excellent performance for the F10.7 and Dst indices and good predictive accuracy for the K_p and ap indices, while the AE index remained the most challenging target because of its highly dynamic behavior. An important advantage of this study is that accurate predictions are obtained using a single, long-term measure of solar activity together with a small set of engineered features. This makes the proposed method computationally efficient and applicable to historical datasets where detailed solar-wind measurements may not be available. Future work will focus on integrating additional solar observations and in situ solar-wind parameters to improve the prediction of rapidly evolving geomagnetic disturbances and significant solar phenomena. Extending the framework to multi-step and probabilistic forecasting also represents a promising direction for future research in observational astronomy and basic space science.

Acknowledgment

The authors gratefully acknowledge the NASA OMNIWeb database for providing the high-resolution space physics data used in this study. The authors also acknowledge the use of artificial intelligence tools for language editing and improving the clarity of the manuscript.

Authors' Contributions

All authors have contributed equally to the conceptualization, methodology, software development, and writing of this manuscript.

Data Availability

The historical relative sunspot number, solar radio flux, and geomagnetic index data that support the findings of this study are openly available in the NASA OMNIWeb database at `https://omniweb.gsfc.nasa.gov/`.

Conflicts of Interest

The authors declare that there is no conflict of interest regarding the publication of this paper.

Ethical Considerations

The authors have diligently addressed ethical concerns, such as informed consent, plagiarism, data fabrication, misconduct, falsification, double publication, redundancy, submission, and other related matters.

Funding

This research did not receive any specific grant from funding agencies in the public, commercial, or not for profit sectors.

References

[1] Hood, A. W., & Hughes, D. W. 2011, Physics of the Earth and Planetary Interiors, 187, 78, special Issue: Planetary Magnetism, Dynamo and Dynamics.

[2] Wiegelmann, T., Thalmann, J. K., & Solanki, S. K. 2014, A&A Rev., 22, 78.

[3] Charbonneau, P. 2014, ARA&A, 52, 251.

[4] Clette, F., et al. 2007, Advances in Space Research, 40, 919.

[5] Hathaway, D. H. 2010, Living Reviews in Solar Physics, 7, 1.

[6] Clette, F., Svalgaard, L., Vaquero, J. M., & Cliver, E. W. 2014, Space Sci. Rev., 186, 35.

[7] Schwabe, H. 1844, Astronomische Nachrichten, 21, 233.

[8] Hale, G. E. 1908, ApJ, 28, 315.

[9] Mayaud, P.-N. 1972, J. Geophys. Res., 77, 6870.

[10] Bergin, A., Chapman, S., Gjerloev, J., & Watkins, N. 2019, EGU General Assembly Conference Abstracts, EGU General Assembly Conference Abstracts.

[11] Echer, E., Gonzalez, W. D., Tsurutani, B. T., & Gonzalez, A. L. C. 2008, J. Geophysical Research (Space Physics), 113, A05221.

[12] Verbanac, G., Mandea, M., Vršnak, B., & Sentic, S. 2011, Sol. Phys., 271, 183.

[13] Webb, D. 1995, Advances in Space Research, 16, 57.

[14] Richardson, I. G., Cliver, E. W., & Cane, H. V. 2000, J. Geophys. Res., 105, 18,203.

[15] Tsurutani, B. T., et al. 2006, J. Geophysical Research (Space Physics), 111, A07S01.

[16] Ohl, A. I. Forecast of Sunspot Maximum Number of Cycle 20, 1966, in Russian.

[17] Ohl, A. I., & Ohl, G. I. 1979, NOAA Solar-Terrestrial Predictions Proceedings. Volume 2.

[18] Feynman, J. 1982, J. Geophys. Res., 87, 6153.

[19] Hathaway, D. H., & Wilson, R. M. 2006, Geophysical Research Letters, 33.

[20] Petrovay, K. 2020, Living Reviews in Solar Physics, 17, 2.

[21] Echer, E., et al. 2004, J. Atmospheric and Solar-Terrestrial Physics, 66, 1019.

[22] Falayi, E. O., & Rabiu, B. A. 2013, Acta Geophysica, 61, 211.

[23] Arora, K., Chandrasekhar, N. P., Nagarajan, N., & Singh, A. 2014, J. Atmospheric and Solar-Terrestrial Physics, 114, 19.

[24] Singh, Y. P., & Badruddin 2014, Planet. Space Sci., 96, 120.

[25] Rathore, B., et al. 2012, Indian J. Physics, 86, 563.

[26] 2018, Machine Learning Techniques for Space Weather, , edited by Camporeale, E., Wing, S., & Johnson, J. R. Elsevier.

[27] Camporeale, E. 2019, Space weather, 17, 1166.

[28] Camporeale, E., & of ML-Helio, S. O. C. 2020, J. Geophysical Research: Space Physics, 125, e2019JA027502.

[29] Kitiashvili, I. N., et al. 2020, SAO/NASA Astrophysics Data System.

[30] Upendran, V., et al. 2022, Space Weather, 20, e2022SW003045.

[31] Nair, M., et al. 2023, Space Weather, 21, e2023SW003514.

[32] Guastavino, S., et al. 2024, The Astrophysical Journal, 971, 94.

[33] LI, S., et al. 2025, Chinese J. Space Science, 45, 641.

[34] Ranjbar, S., & Taran, S. 2026, IJAA, 12, 323.

[35] Friedli, T. K. 2016, Sol. Phys., 291, 2505.

[36] NOAA National Centers for Environmental Information Geomagnetic Indices and Data, `https://www.ncei.noaa.gov/products/geomagnetic-indices`, 2026, accessed 2026-07-15.

[37] Tapping, K. 2013, Space weather, 11, 394.

[38] Hathaway, D. H. 2015, Living reviews in solar physics, 12, 4.

[39] Gonzalez, W., et al. 1994, J. Geophysical Research: Space Physics, 99, 5771.

[40] Kivelson, M. G., & Russell, C. T. 1995, Introduction to Space Physics, Cambridge University Press.

[41] Hathaway, D. H. 2015, Living Reviews in Solar Physics, 12, 4.

[42] Wang, R., Wang, J., Liang, T., & Zhang, H. 2024, Space Weather, 22, e2024SW004002.

[43] Pulkkinen, T. 2007, Living Reviews in Solar Physics, 4, 1.